The Journal of the Acoustical Society of America

APRIL 29 2019

Acoustic impedance of micro-perforated panels in a grazing flow

Xiaoqi Zhang; Li Cheng

Check for updates

J. Acoust. Soc. Am. 145, 2461–2469 (2019)
https://doi.org/10.1121/1.5098785

View Online
Export Citation
CrossMark

15 February 2024 01:59:50

ASA
LEARN MORE
Advance your science and career as a member of the
Acoustical Society of America

ASA
ACOUSTICAL SOCIETY OF AMERICA

CrossMark click for updates

Acoustic impedance of micro-perforated panels in a grazing flow

Xiaoqi Zhang and Li Cheng[a)]
Department of Mechanical Engineering, The Hong Kong Polytechnic University, Kowloon, Hong Kong, China

(Received 3 January 2019; revised 2 April 2019; accepted 2 April 2019; published online 29 April 2019)

Micro-perforated panels (MPPs) are widely used for broadband sound absorptions. For a MPP exposed to a grazing flow, existing acoustic impedance formulas based on different flow parameters give inconsistent results, thus calling for a systematic investigation of the issue to find more intrinsic flow parameters allowing for a reliable acoustic impedance prediction. In this study, three-dimensional CFD simulations are conducted on a MPP hole with a backing space in a flow duct. Numerical results allow identifying the flow velocity gradient in the viscous sublayer as the intrinsic flow parameter and show its linear relationship with a flow-related term in the acoustic resistance formula. Through a linear regression analysis, an acoustic resistance formula is established within a certain flow range (Mach number up to 0.25) under the linear acoustic regime. The validity of the impedance formula is demonstrated through comparisons with existing results and experimental data reported in the literature, showing good agreement and superiority in terms of the prediction accuracy. © *2019 Acoustical Society of America*.
https://doi.org/10.1121/1.5098785

[NX] Pages: 2461–2469

I. INTRODUCTION

A micro-perforated panel (MPP) is a thin sheet with perforations over its surface. With the hole size typically in the sub-millimeter range, a MPP provides a high acoustic resistance (loss) and a low acoustic reactance (mass) by the structure itself, conducive to effective sound absorption with a proper design. Owing to their unique and environmentally friendly nature, MPPs are being widely used in various noise control applications as an alternative to traditional porous/fibrous sound absorption materials.

The acoustic property of a MPP can be characterized by its surface impedance. Based on the work of Lord Rayleigh[1] and Crandall,[2] Maa proposed various forms of acoustic impedance prediction formulas by considering a MPP as a lattice of short tubes with end corrections.[3,4] Since then, research on MPPs has been intensifying, as evidenced by the large amount of papers published on the topics, ranging from the design of various types of MPP absorbers to the exploration of their applications.[5,6] In addition to the conventional architectural and environmental acoustic problems,[7] their applications in compact mechanical systems[8,9] start to draw increasing attention. Affected by the surrounding acoustic environment, MPPs behave very differently from the simple laboratory setting, thus requiring their consideration as an integral part of the entire acoustic/vibro-acoustic system.[10,11]

In addition to problems in a still acoustic medium, an important category of MPP problems involves flow, among which the case of the grazing flow is probably the most representative and practically important. Typical examples include vehicle exhaust silencers, flow duct linings, or various types of domestic products.

Existing work relating to the flow passing through a perforated hole in a plate has been arousing wide interest. Theoretical[12–16] or semi-theoretical models[17,18] were developed upon making different simplifications on the interactions between the acoustic waves and the flow field near the perforated holes. While shedding light on the underlying physics, most of these theoretical or semi-theoretical models only consider inviscid flow for a hole size which is beyond micro-perforated range. Meanwhile, due to the problem simplification, the predicted acoustic impedance only qualitatively agrees with experimental data.[19] A continuous effort is to develop empirical models for the acoustic impedance prediction.[19–30] To this end, identifying the key flow parameters which are intrinsically linked to the acoustic impedance of the hole is the critical component. Observing the inconsistencies in the prediction results,[19] studies point at the necessity of considering boundary layer parameters to characterize the grazing flow effects. When the boundary layer is thicker than the orifice diameter, the inner boundary layer parameters need to be included as suggested by Cummings.[26]

Most of the aforementioned studies considered perforations with a hole diameter typically around 1 mm or larger. This, in a strict sense, falls beyond the scope of the micro-perforation in the perspective of achieving sound absorption. More relevant to the micro-perforation investigated in the present paper is the work of Allam and Åbom[24] in which an impedance formula was developed using the Mach number as the flow parameter.

With the fast development of the computational capability, numerical methods such as DNS, LES, and RANS are more frequently used to investigate these problems.[31–37] For example, DNS was applied to a single Helmholtz resonator to understand its sound energy dissipation mechanism.[31–33] Results indicated a transition from the viscous-dominant

[a)]Electronic mail: li.cheng@polyu.edu.hk

15 February 2024 01:59:50

dissipation in the shear layer near the hole to the chaotic vortex shedding dominant dissipation with the increasing sound pressure level (SPL). It was shown that,[35–37] without using the highly computationally costly methods like LES or DNS, more cost-effective tools like three-dimensional (3D) URANS CFD could reasonably predict the acoustic behavior of the Helmholtz resonator[35] and the perforated panel silencers[36] in both no-flow and flow conditions.

Existing work allowed a qualitative description of the acoustic behavior of MPPs in the presence of a grazing flow. Different from the no-flow condition, however, a universally accepted and consistent acoustic impedance formula to guide the practical design of MPPs in the presence of flow is still lacking. The intrinsic flow parameters which can intrinsically characterize the inherent grazing flow effects on the acoustic impedance of MPPs still need to be found.

Motivated by this, the present paper investigates the acoustic behavior of MPPs under fully developed turbulent grazing flow conditions within the linear acoustic regime. The main focuses are put on three aspects. (1) The flow field around the holes of a MPP is scrutinized and investigated. (2) A new flow parameter which intrinsically relates the grazing flow effects with the acoustic impedance of the MPP is identified. (3) A new impedance prediction formula is proposed to supplement the one by Maa in the no-flow condition.[4]

More specifically, numerical studies are carried out through 3D URANS CFD simulations. Computed results are then presented for validating the CFD model, identifying the new intrinsic flow parameter and establishing the impedance formula. Prediction results from the proposed formula are then compared with those from other existing formulas or experimentally measured data to show the accuracy and the improvement that the new impedance formula brings about.

II. COMPUTATIONAL MODEL AND SIMULATION METHOD

A. Model

Consider a MPP panel with a honeycomb backing cavity. Each hole in the face plate and the cavity cell behind it forms a Helmholtz resonator (Fig. 1). The entire honeycomb MPP absorber can be regarded as an assembly of an array of Helmholtz resonators. We assume a low perforation ratio (typically around 1%) so that each resonator would act independently and the interaction between the holes is therefore neglected. Under this condition, the acoustic impedance of the panel is equal to that of a single isolated MPP hole divided by the perforation ratio. The computational model will use a single Helmholtz resonator, shown in Fig. 1.

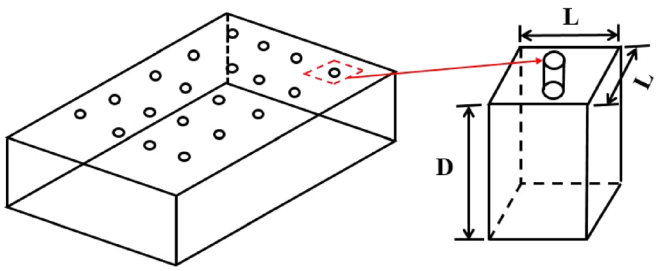

FIG. 1. (Color online) Perforated panel (left) modeled by a single Helmholtz resonator (right).

Geometrical parameters of MPPs being investigated hereafter are listed in Table I. All panels used for simulations and comparisons, both numerically and experimentally, are typical MPPs (with hole diameters smaller than 1 mm). Note that Panel 1, with cylindrical holes of a diameter $d = 0.68$ mm, is the configuration used by Malmary *et al.*[38] All panels have the same size of 24×24 mm, with a 10 mm deep backing cavity, same as Ref. 38. The side length of each MPP cell, L, is determined based on the perforation ratio, giving $L = 5.12$ mm.

The modelled system is shown in Fig. 2 (two-dimensional view). A MPP cell is flush-mounted on one sidewall of a square duct with a cross section of 24×24 mm. The upstream portion of the duct is 1000 mm long, which allows the flow to be fully developed. The downstream portion contains two acoustic wavelengths as suggested by Ref. 39.

The computational domain is discretized by multi-size grids, by using structured and unstructured meshes for the duct and the backing cavity, respectively. Denser meshes are used in the region near the orifice and the wall of the duct. Away from these regions, the mesh size increases gradually. To ensure an accurate description of the flow field near the wall, the mesh size of the first layer adjacent to the duct wall was designed to ensure that $y^+ = yU_\tau/\nu \leq 1$, in which U_τ is the friction velocity, y is the distance from the first layer mesh to the wall in the normal wall direction, and ν is the kinematic viscosity of the air.

Inside the hole, the average size of the elements is 0.015 mm. In the duct, the grid spacing in the stream-wise direction ranges from 0.015 to 1.6 mm upstream the resonator and from 0.015 to 2.4 mm downstream, which results in a minimum of about 65 and 43 grids per acoustic wavelength upstream and downstream the resonator, respectively, at the highest frequency considered in the study. The grid spacing in the normal wall and span-wise direction ranges from 0.0075 to 1 mm and from 0.015 to 0.8 mm, respectively. This results in a total of about 3 000 000 elements. The convergence of the solution in relation to meshing is conducted through investigating the time-domain variation of acoustic pressure and velocity at the hole inlet section, which are used to calculate the acoustic impedance of the hole. Results indicate that convergence can be achieved to the accuracy needed for impedance prediction.

B. Computational method

The 3D URANS is adopted using the commercial CFD code, FLUENT. The choice of the simulation tool is justified

TABLE I. Geometry parameters of the MPPs, Plate 1 is taken from Ref. 38.

Panel number	Orifice diameter d (mm)	Panel thickness t (mm)	t/d	Perforated ratio δ
1	0.68	1.02	1.7	1.39%
2	0.5	1.02	2.04	1.39%
3	0.3	0.3	1	1.39%

15 February 2024 01:59:50

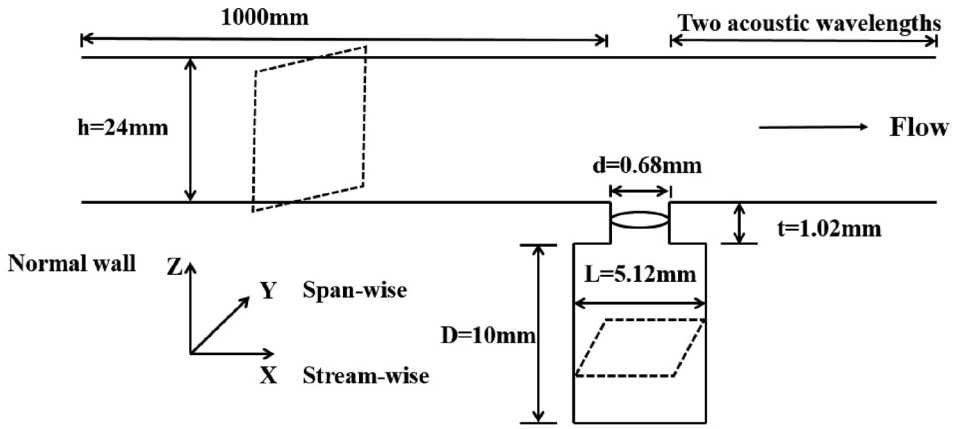

FIG. 2. System model.

by the observations made in previous work on acoustic attenuators.[35–37] The mass flow rate boundary condition is applied to the inlet of the duct. The pressure at the outlet is set to be the atmospheric pressure. Solid wall boundary conditions with no slip are imposed to all wall surfaces. A pressure-based implicit solver is employed. The pressure-velocity coupling scheme Pressure-Implicit with Splitting of Operators algorithm is applied for both the stable mean flow field and the aero-acoustic coupling simulation. The second order scheme is chosen for both the spatial discretization and time integration. The number of unknowns in the equations of URANS is more than that of the equations. These equations are unclosed. The Realizable k - ε turbulence model is adopted for this closure problem.

A two-step approach is used to deal with the interaction between the flow and the acoustic wave near the hole. The stable mean flow field is first computed. Harmonic acoustic waves with a given velocity amplitude are then added as the acoustic excitation. The stable mean grazing flow is calculated by running the unsteady solver until flow properties stop changing. The time step size for the stable mean flow computation is 5×10^{-6} s. That used in acoustic simulations is 5×10^{-7} s.

III. CFD MODEL VALIDATION

The viscous sub-layer region adjacent to the flow field in the hole plays a key role in the acoustic impedance of the hole. The velocity gradient in this layer and the friction velocity are important parameters in this near-wall region. They are first investigated to ensure a truthful description by the CFD model.

A. Mean stream-wise velocity

To check the quality of the flow simulation, the mean stream-wise velocity profiles at two upstream locations at $M = 0.25$ are shown in Fig. 3. The origin of coordinates was set at the center of the inlet surface of the MPP cell. The observed same profiles demonstrate that the flow is fully developed before reaching the MPP cell.

The corresponding semi-log plots of the mean stream-wise velocity at $x = -50$ mm is shown in Fig. 4, along with the well-known logarithmic law.[40] In the figure, $U^+ = \langle U \rangle / U_\tau$, $\langle U \rangle$ is the mean stream-wise velocity. It can be seen that the predicted data agree well with the empirical equation,[40] including the viscous sublayer region ($y^+ \leq 5$) where the CFD data follow quite well with the well-known trend $U^+ = y^+$.

B. Friction velocity

As to be demonstrated later, the acoustic impedance of the MPPs under grazing flow is well correlated to the

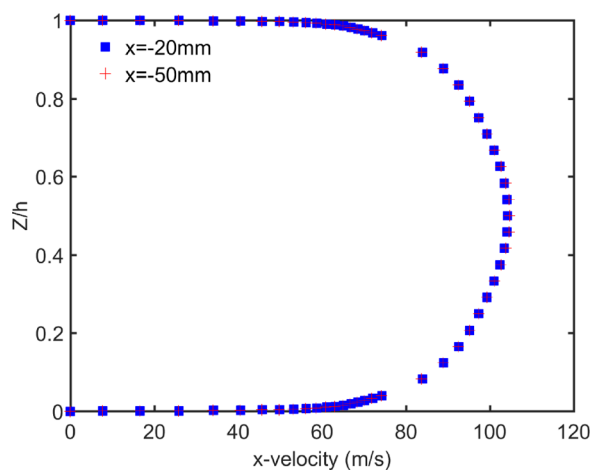

FIG. 3. (Color online) Mean x-velocity profiles at different locations upstream the resonator, through the $y = 0$ cross section. $M = 0.25$.

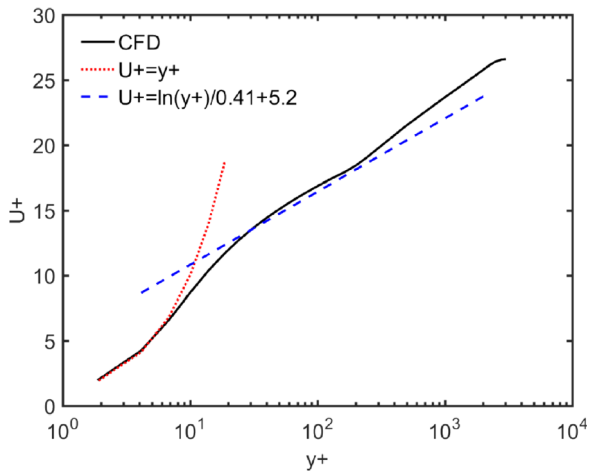

FIG. 4. (Color online) Semi-log plots of the mean stream-wise velocity profile upstream the resonator at $x = -50$ mm, through $y = 0$ cross section. $M = 0.25$.

15 February 2024 01:59:50

velocity gradient in the viscous sublayer over the duct wall, G, defined as

$$G = \frac{U_\tau^2}{v}, \tag{1}$$

with the friction velocity, U_τ, calculated by

$$U_\tau = \sqrt{\frac{\tau_w}{\rho}}, \tag{2}$$

where ρ is the air density, τ_w is the wall shear stress, which can be determined from the free-stream grazing flow velocity U and the Darcy friction factor as

$$\tau_w = \frac{\rho U^2 \lambda}{8}. \tag{3}$$

The expression developed by Fujita[41] is used to calculate λ whose accuracy is shown to be within engineering accuracy[19]

$$\lambda = \frac{0.178}{R_e^{1/5}}, \tag{4}$$

where $R_e = hU/v$ is the Reynolds number with h being the height of the square duct.

The numerically calculated friction velocity is compared with the prediction by the empirical equation,[41] as shown in Fig. 5. The agreement between the two sets of results demonstrate the validity of the computational model.

C. Acoustic impedance simulation and comparisons with experiments

The accuracy of the CFD model to predict the acoustic impedance of MPPs in the presence of grazing flow is validated through comparisons with experimental data reported in the literature.

The normalized acoustic impedance of a MPP hole is defined as

$$Z_{\text{hole}} = \frac{1}{\rho c}\frac{P_{\text{in}} - P_{\text{out}}}{\bar{u}}, \tag{5}$$

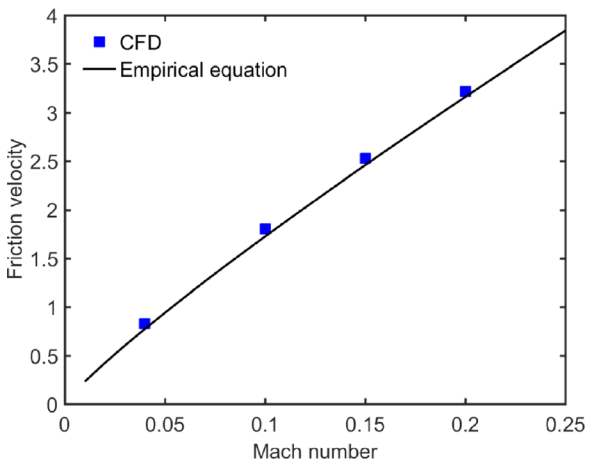

FIG. 5. (Color online) Comparison of the friction velocity between CFD and the empirical equation (Ref. 41).

TABLE II. Computational cases.

Mach number	0.04	0.08	0.1	0.15	0.16	0.2	0.25
R_e	21 108	43 271	52 769	79 153	84 430	105 538	131 923

where c is the speed of sound in air, P_{in} and P_{out} are the space-averaged acoustic pressure over the inlet and outlet surface of the hole, respectively, and $\bar{u}$ is the space-averaged acoustic velocity normal to the hole cross-section. Since the acoustic wavelength is much larger than the thickness of the hole, the normal acoustic velocities at both sides of the hole can be assumed to be the same.

The normalized acoustic impedance of the entire MPP can then be obtained by

$$Z = \frac{Z_{\text{hole}}}{\delta} = R + j\chi, \tag{6}$$

where R and χ are the normalized acoustic resistance and reactance, respectively.

Fast Fourier transform is performed on the stable cycles of the related time signals, and their complex values at the acoustic frequency are determined.[39] Using Eqs. (5) and (6), the normalized acoustic impedance of MPP is then deduced.

The acoustic behavior of Panel 1 under different flow speeds is first investigated, for a Mach number varying from 0.04 to 0.25 and an acoustic excitation at 111 dB at 3150 Hz. Note this frequency is chosen to enable comparisons with the data provided in Ref. 38. The Mach numbers alongside the corresponding Reynolds numbers of the computation cases are listed in Table II.

The acoustic impedance of Panel 1 obtained from the CFD simulations and from experimental measurements,[38] is compared in Fig. 6. Both sets of results show that the acoustic resistance increases with the Mach number, while the reactance decreases. It can also be seen that the experimentally observed trend and the magnitude of the impedance

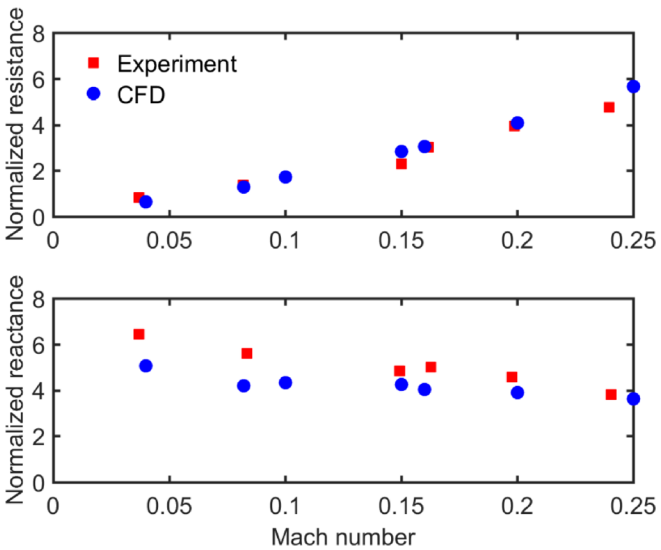

FIG. 6. (Color online) Comparison of the normalized acoustic impedance of Panel 1 between CFD and experiments.

15 February 2024 01:59:50

terms are reasonably well reproduced by the CFD simulations.

Note that in the no-flow case, an end correction term appears in the reactance part in Eq. (6) to count for the effective mass flowing through the hole. This, however, is difficult to be precisely determined in the present case, which apparently depends on the flow conditions. The end-correction, however, is not necessary to the resistance part with flow, since dissipation mainly takes place inside the hole. It is also pertinent to note that previous works[16,18,24] have shown that, with grazing flow, the acoustic resistance is insensitive to frequency variation (also confirmed in the following analyses). Therefore, the comparison, though at only one frequency, is deemed representative enough.

The above validations confirm the validity of the acceptable accuracy of the proposed CFD model, which is to be used for flow analyses and the development of the acoustic impedance prediction formula.

IV. FLOW FIELD VISUALIZATIONS AND ANALYSES

A. Flow field at different Mach numbers

Analyses on the flow field near the MPP aperture and inside the hole would help to better understand the physical process of the flow-acoustic-MPP interaction. To this end, the case without acoustic excitation is first examined. Figure 7 shows the velocity streamlines of the mean grazing flow near the hole of the resonator at different Mach numbers. It can be seen that the flow passes over the hole with no visible fluid flowing into or out of the cavity through the hole, along with the formation of a shear layer above it. The grazing flow induces an additional flow motion inside the hole by the shear stress transmitted through the hole in the wall. At a low Mach number of $M = 0.04$, two vortical flow regions in the hole are observable. In the upper region a big vortex with clockwise rotation is formed, entraining a smaller one in the lower area with counter clockwise rotation. The vortices together with the small hole would prevent the fluid entrainment through the hole. When the flow velocity increases, the smaller vortex in the lower part of the hole disappears while the upper vortical flow region grows, leading to an increase in the contacting area between the vortical flow and the wall of the hole.

Acoustic excitation is then added. As an example, the velocity streamlines near the hole with an acoustic excitation defined in Sec. III C are shown in Fig. 8. It can be seen that, at a very low Mach number of $M = 0.04$, different from the sole mean grazing flow case (Fig. 7), fluid is entrained into the cavity. Meanwhile, the vortex in the upper area of the hole becomes smaller and the small vortex in the lower area of the hole with counter clockwise rotation disappears, as compared with the case without acoustic excitation (Fig. 7). However, the effect of the acoustic excitation on the global flow field is not obvious at other flow velocities. This can be explained by the fact that the size of the vortex in the hole gradually grows with the flow speed, along with an increase of the resistant effect of the vortex in the hole. In the present case, the acoustic energy is not strong enough to overcome the resistant effect of the vortex in the hole at high flow

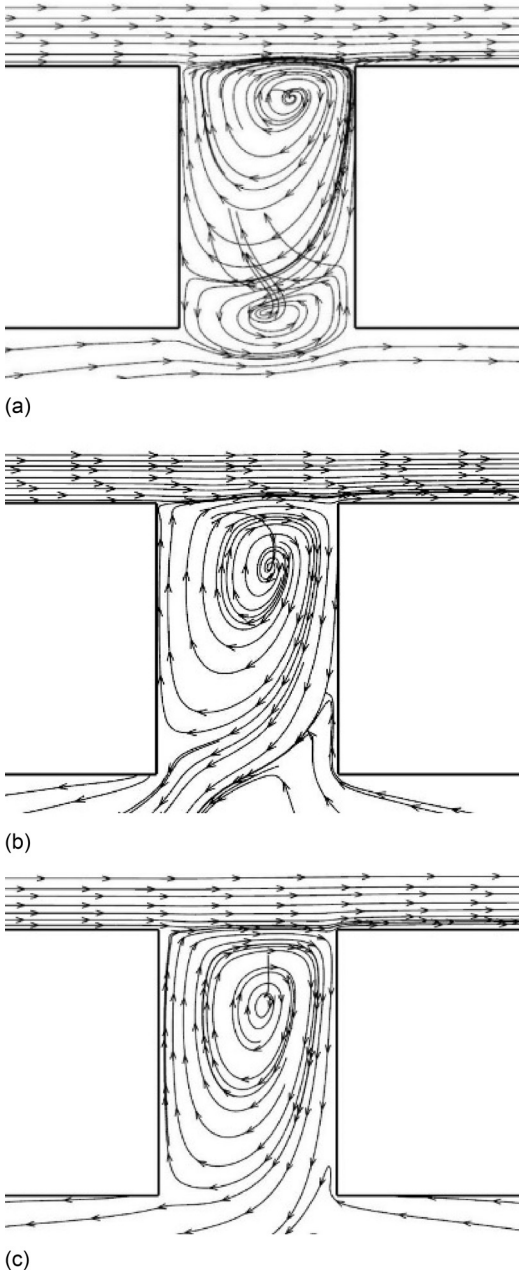

FIG. 7. Velocity streamlines of mean grazing flow near the hole of the resonator through $y = 0$ cross section at different flow Mach numbers. (a) $M = 0.04$, (b) $M = 0.1$, and (c) $M = 0.25$.

velocities. As a result, unlike the case of $M = 0.04$, there is no fluid flowing into the cavity, and the streamline pattern near the hole is almost the same as the case without acoustic excitation. The observed flow pattern also echoes with the common belief that viscous dissipation in the shear layer of the hole dominates the sound absorption mechanism at this typical SPL level.

B. Intrinsic flow parameters for acoustic impedance prediction

The flow field near the hole can be seen as a superposition of the oscillating flow field caused by the acoustic excitation and the grazing flow. It can be surmised that the flow parameter which can best determine the flow field near the

15 February 2024 01:59:50

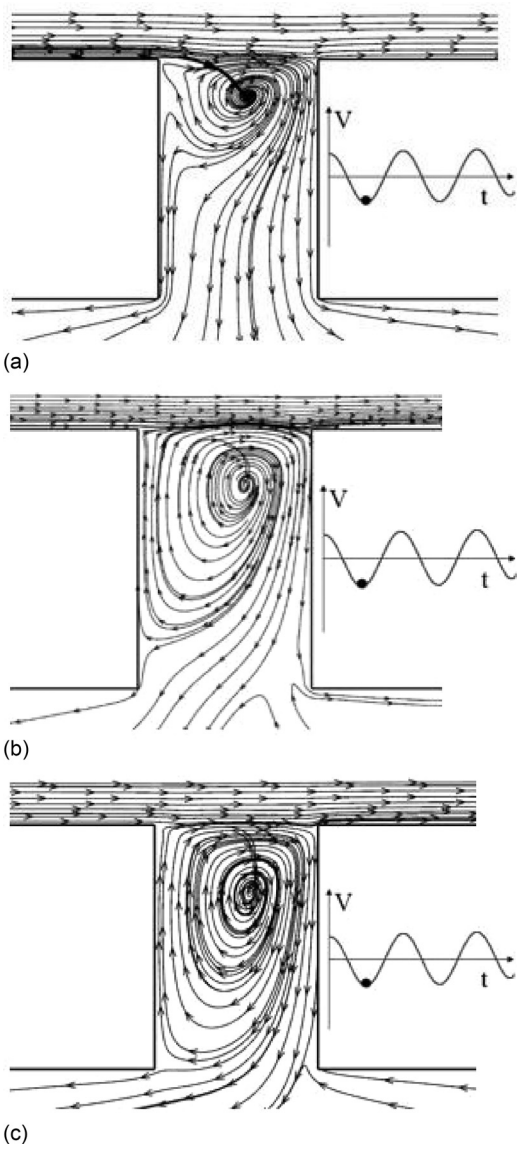

FIG. 8. Velocity streamlines near the hole of the resonator through $y=0$ cross section at different flow velocities. $f=3.15$ kHz, $|V_a|=0.025$ m/s. (a) $M=0.04$, (b) $M=0.1$, and (c) $M=0.25$.

hole would influence the acoustic impedance of the MPP holes. An enlightening example is the case of a linear shear flow passing over a plane wall with a circular hole, generating the so-called Stokes flow near the hole,[42–46] in which case the local Reynolds number based on the diameter of the orifice is smaller than 1. The exact solution by Davis[46] suggests that the velocity gradient of the linear shear flow might be the key parameter which determines the distribution of the velocity and pressure near the hole. Enlightened by the work of Davis,[46] we propose the flow velocity gradient in the viscous sublayer as the new flow parameter, and subsequently establish its link to the acoustic impedance of the MPP hole. The choice of the velocity gradient is also supported by the flow field analyses, reported in Sec. IV A. With the viscous sublayer being adjacent with the flow field in the hole, the velocity gradient in this layer produces the shear stress, responsible for the flow pattern in the hole as well as the acoustic energy dissipation.

V. IMPEDANCE PREDICTION MODEL

A. Relationship between the velocity gradient and the acoustic resistance of MPPs

To establish the relationship between the velocity gradient in the viscous sublayer over duct wall, denoted by G, and the acoustic resistance of MPPs under a grazing turbulent flow, numerical experiments are curried out. Panel 1, the same one used in Ref. 38, is first investigated. After finding the relationship between the velocity gradient in the viscous sublayer and the acoustic resistance of this panel, other panels will be used for further verifications. For each panel, additional computational cases are considered with details tabulated in Table III. In each case, the panel is exposed to the same flow speed range and acoustic excitation level as before, but at different frequencies.

In the no-flow case, the normalized acoustic resistance of a MPP proposed by Maa[4] writes

$$R = R_{\text{in}} + R_{\text{out}} = \frac{32vt}{\delta c d^2}\left[1+\frac{K^2}{32}\right]^{1/2} + \frac{\sqrt{2}}{32}K\frac{d}{t}, \tag{7}$$

where $K = d\sqrt{\omega/4v}$; R_{in} represents the viscous effects in the hole and R_{out} is the end correction counting for the viscous loss outside the hole.

In the presence of grazing flow, we replace R_{out} with a new term, θ, to count for the viscous loss. Therefore, the normalized acoustic resistance of the MPP, R_{flow}, writes

$$R_{\text{flow}} = R_{\text{in}} + \theta. \tag{8}$$

Both θ and G are non-dimensionalized as $\theta c/fd$ and Gt/fd, respectively. Figure 9 displays the CFD results using Panel 1 at different excitation frequencies ranging from 2400 to 3300 Hz at different flow velocities. The plot is grouped into four groups, each having the same Mach number but different frequencies. The corresponding Mach number varies from 0.1 to 0.25. As observed in Fig. 9, although each group of results seems to have a slightly different slope, there seems to exist a rather linear relationship between the two parameters ($\theta c/fd$ and Gt/fd) which can be reasonably well represented by a straight line. This also confirms that the amended term in the acoustic resistance formula under grazing flow is related to the velocity gradient in the viscous sublayer region.

To further confirm the generality of the observed linear relationship between, two other MPPs (Panels 2 and 3) with different hole dimensions are also examined through CFD simulations (with cases listed in Table III). Results are shown in Fig. 10, which show that, though following a different slope, the linear relationship between $\theta c/fd$ and Gt/fd still holds reasonably well, confirming the general nature of the observations made on Panel 1.

A linear regression analysis is conducted to establish the observed linear relationship as

$$\frac{\theta c}{fd} = A\frac{Gt}{fd} + B, \tag{9}$$

15 February 2024 01:59:50

TABLE III. Computational cases used to find the relation between G and the acoustic resistance.

Velocity amplitude of the incident acoustic wave (m/s)	Frequency (Hz)	Mach number	R_e
$\lvert V_a\rvert = 0.025$	3150, 3000, 2800, 2600, 2400	0.1	52 769
	3300, 3150, 3000, 2800, 2600,	0.15	79 153
	3300, 3150, 3000, 2800, 2600,	0.2	105 538
	3300, 3150, 3000, 2800, 2600,	0.25	131 923

where A and B, as a function of t/d, are to be determined. Curve-fitting the calculated resistance data for panels 1, 2, and 3 leads to the following expression:

$$\frac{\theta c}{fd} = \left[0.0356\left(\frac{t}{d}\right)^{-3.236} + 0.0157\right]\frac{Gt}{\delta fd} + \left[1.369 - 2.331\left(\frac{t}{d}\right)^{-2.195}\right]\frac{1}{\delta}. \quad (10)$$

B. Resistance model of MPPs and validations

Combining Eqs. (8) and (10), a normalized acoustic resistance formula for MPPs under grazing turbulent flow is established as follows:

$$R_{\text{flow}} = R_{\text{in}} + \left[0.0356\left(\frac{t}{d}\right)^{-3.236} + 0.0157\right]\frac{Gt}{\delta c} + \left[1.369 - 2.331\left(\frac{t}{d}\right)^{-2.195}\right]\frac{fd}{\delta c}, \quad (11)$$

where $R_{\text{in}} = (32vt/\delta cd^2)[1 + (K^2/32)]^{1/2}$, with G calculated by Eqs. (1)–(4).

For validation purposes, Fig. 11 shows a comparison of the normalized acoustic resistance between the proposed formula and the experimental data for Panel 1, reported in Ref. 38. Meanwhile, the same comparisons with the CFD data for Panel 1 at other frequencies are also given in Fig. 12 with different Mach numbers. These comparisons clearly show that the proposed formula cannot only capture the trend but also agrees well with both the experimental data and CFD simulations. They also confirm the fact that the resistance is nearly constant and insensitive to frequency variations. Similar conclusions can be drawn for Panels 2 and 3 (not shown here for brevity).

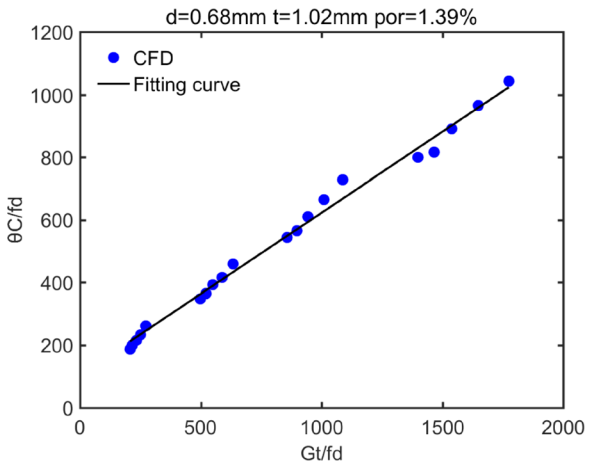

FIG. 9. (Color online) Relationship between θ and G for Panel 1. $|V_a| = 0.025$ m/s.

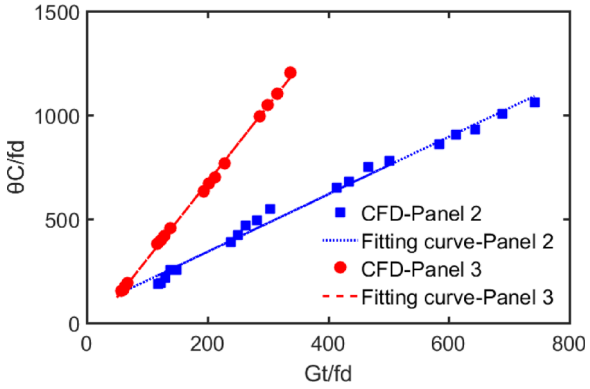

FIG. 10. (Color online) Relationship between θ and G for panels 2 and 3. $|V_a| = 0.025$ m/s.

It should also be pointed out that the above analyses and the proposed acoustic resistance formula are based on a number of selected cases. Therefore, the validity range, as verified in the present study, is limited to $R_e \leq 131\,923$ (corresponding to $M \leq 0.25$ for current cases), $1 \leq (t/d) \leq 2$ and under linear acoustic excitation range.

Additional comparisons with other existing models reported in the literature are finally conducted. To this end, Kirby and Cummings' model[19] and Allam and Åbom's model[24] are used, with results shown in Fig. 13. To facilitate comparisons, experimental data[38] are also provided in the same figure. It can be seen that the prediction results by the present formula seem to fit the measured data better than the other two models. More specifically, compared with Kirby and Cummings' model, the present model seems to work better, especially at a low Mach number range before 0.1. In

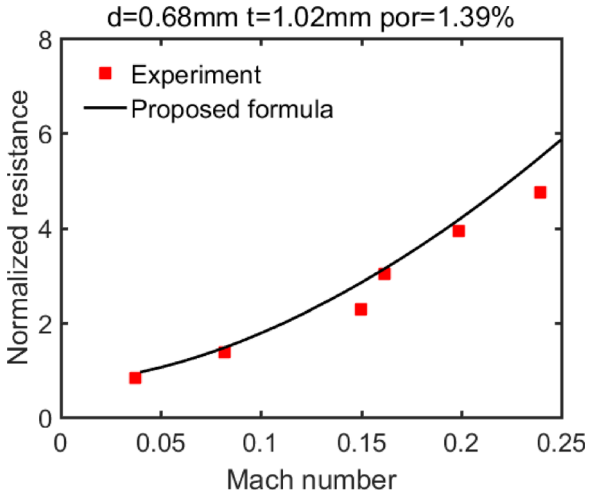

FIG. 11. (Color online) Normalized acoustic resistance comparisons between proposed formula and experimental data for panel 1. $f = 3.15$ kHz, $|V_a| = 0.025$ m/s.

15 February 2024 01:59:50

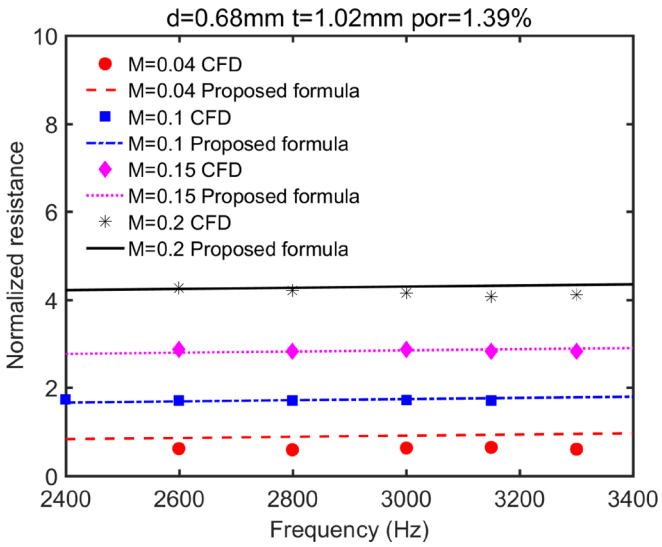

FIG. 12. (Color online) Normalized acoustic resistance comparisons between proposed formula and CFD for panel 1. $|V_a| = 0.025\,\mathrm{m/s}$.

the higher Mach number region, the proposed formula follows better experimental data than Allam and Åbom's model. Over the entire region, the proposed model can capture the nonlinearly increasing trend of the acoustic resistance.

As mentioned before, both previous work[16,18,24] and the CFD simulations in Fig. 12 show that, with grazing flow, the acoustic resistance is roughly independent of frequency. Therefore, the experimental data found in literature, though at one frequency, is rather representative. Similarly, the limited cases being investigated in the paper actually cover a much wider scope and are applicable for a range of different frequencies. However, considering the very scarce experimental research on MPPs with low grazing flow velocity under the linear acoustic excitation region, more experiments will be carried out in our future work.

As a final remark, it should be noted that the above analyses heavily focus on the acoustic resistance part of the impedance formula. To complete the acoustic impedance prediction, the proposed resistance formula can be combined with the acoustic reactance prediction model proposed by Cummings,[26] which was tested to show a rather good consistency against the experimental results on Panel 1 (results not shown here for brevity). Casting Cummings' reactance formula by using parameter G proposed in this paper is straightforward. Combined with Eq. (11), a complete set of the acoustic impedance prediction formulas for MPPs with grazing flow within the linear acoustic regime is established.

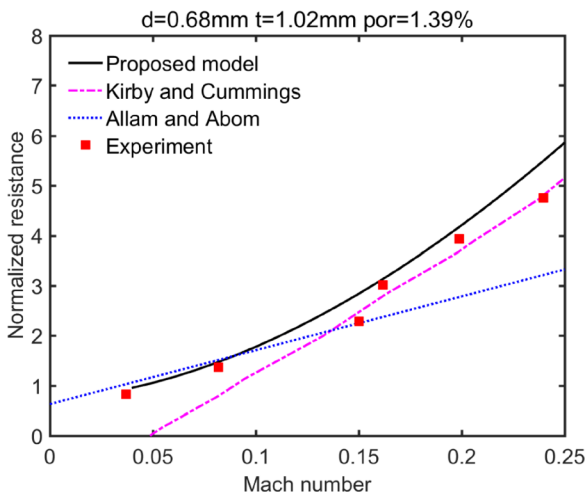

FIG. 13. (Color online) Comparisons between the proposed formula with that of Kirby and Cummings (Ref. 19) and that of Allam and Åbom (Ref. 24) for panel 1. $f = 3.15\,\mathrm{kHz}$, $|V_a| = 0.025\,\mathrm{m/s}$.

VI. CONCLUSIONS

The acoustic behavior of MPPs, exposed to fully developed grazing turbulent flow, is investigated through numerical simulations. Grazing flow and acoustic wave-excited flow field near the orifice of the MPP under different flow conditions is scrutinized through solving the compressible Reynolds averaged Navier–Stokes equations.

Based on the analyses of the flow field near the MPP orifice, the velocity gradient in the viscous sublayer over the duct wall is identified as the intrinsic flow parameter which is inherently related to the acoustic resistance of the MPPs with grazing flow. Numerical results reveal its linear relationship with the flow-related part in the acoustic resistance formula. Based on this, a new resistance formula is proposed, which is shown to be applicable at a Mach number up to roughly 0.25 under the linear acoustic excitation regime. The accuracy and superiority of the model as compared with the existing ones are demonstrated through comprehensive comparisons with the data provided in the open literature. It is shown that the proposed formula agrees well with the experimental data and outperforms existing models in terms of both prediction accuracy and application range. Combined with Cummings' reactance model, a complete set of the acoustic impedance prediction formula for MPPs with grazing flow is established.

ACKNOWLEDGMENTS

The authors thank the support from Research Grant Council of the Hong Kong SAR (PolyU 152036/18 E).

[1]R. Lord, *The Theory of Sound II* (MacMillan, New York, 1929), 327 pp.
[2]I. B. Crandall, *Theory of Vibrating Systems and Sound* (Van Nostrand, New York, 1926), 229 pp.
[3]M. Dah-You, "Theory and design of microperforated panel sound-absorbing constructions," Sci. Sin. **18**(1), 55–71 (1975).
[4]D.-Y. Maa, "Potential of microperforated panel absorber," J. Acoust. Soc. Am. **104**(5), 2861–2866 (1998).
[5]K. Sakagami, K. Matsutani, and M. Morimoto, "Sound absorption of a double-leaf micro-perforated panel with an air-back cavity and a rigid-back wall: Detailed analysis with a Helmholtz–Kirchhoff integral formulation," Appl. Acoust. **71**(5), 411–417 (2010).
[6]Y. Wuzhou, "Design and noise reduction of elevated road barrier of micro-perforated panels with linear-change cavity," Environ. Pollution Control **7**, 67–69 (2008).
[7]J. Kang and M. Brocklesby, "Feasibility of applying micro-perforated absorbers in acoustic window systems," Appl. Acoust. **66**(6), 669–689 (2005).
[8]R. Corin and L. Weste, *Sound of Silence* (iVT International, United Kingdom, 2005), pp. 105–107.

15 February 2024 01:59:50

[9]G. Li and C. K. Mechefske, "A comprehensive experimental study of micro-perforated panel acoustic absorbers in MRI scanners," Magn. Reson. Med. **23**(3), 177–185 (2010).
[10]L. Maxit, C. Yang, L. Cheng, and J.-L. Guyader, "Modeling of micro-perforated panels in a complex vibro-acoustic environment using patch transfer function approach," J. Acoust. Soc. Am. **131**(3), 2118–2130 (2012).
[11]C. Yang and L. Cheng, "Sound absorption of microperforated panels inside compact acoustic enclosures," J. Sound Vib. **360**, 140–155 (2016).
[12]E. J. Rice, "Theoretical study of the acoustic impedance of orifices in the presence of a steady grazing flow," J. Acoust. Soc. Am. **59**(S1), S32–S32 (1976).
[13]D. Ronneberger, "The acoustical impedance of holes in the wall of flow ducts," J. Sound Vib. **24**(1), 133–150 (1972).
[14]M. Howe, M. Scott, and S. Sipcic, "The influence of tangential mean flow on the Rayleigh conductivity of an aperture," Proc. Royal Soc. A **452**(1953), 2303–2317 (1996).
[15]X. Jing, X. Sun, J. Wu, and K. Meng, "Effect of grazing flow on the acoustic impedance of an orifice," AIAA J. **39**(8), 1478–1484 (2001).
[16]B. Walker and A. Charwat, "Correlation of the effects of grazing flow on the impedance of Helmholtz resonators," J. Acoust. Soc. Am. **72**(2), 550–555 (1982).
[17]A. Hersch and B. Walker, "Effect of grazing flow on the acoustic impedance of Helmholtz resonators consisting of single and clustered orifices," J. Acoust. Soc. Am. **72**(2), 642–642 (1982).
[18]T. Rogers and A. Hersh, "The effect of grazing flow on the steady state resistance of square-edged orifices," in *Proceedings of the Second AIAA Aeroacoustics Conference* (1976).
[19]R. Kirby and A. Cummings, "The impedance of perforated plates subjected to grazing gas flow and backed by porous media," J. Sound Vib. **217**(4), 619–636 (1998).
[20]B. Phillips, "Effects of high-wave amplitude and mean flow on a Helmholtz resonator," NASA Technical Memorandum X-1582 (1968).
[21]A. B. Bauer, "Impedance theory and measurements on porous acoustic liners," J. Aircraft **14**(8), 720–728 (1977).
[22]L. Dean, "Coupling of Helmholtz resonators to improve acoustic liners for turbofan engines at low frequency," Technical Report, NASA-CR-134912 (1975).
[23]T. Elnady and H. Bodén, "An inverse analytical method for extracting liner impedance from pressure measurements," in Proceedings of the 10th AIAA/CEAS Aeroacoustics Conference, Manchester, United Kingdom (May 2004), pp. 10–12.
[24]S. Allam and M. Åbom, "Experimental characterization of acoustic liners with extended reaction," in The 14th AIAA/CEAS Conference (2008), Vol. 3074.
[25]J. Kooi and S. Sarin, "An experimental study of the acoustic impedance of Helmholtz resonator arrays under a turbulent boundary layer," in *AIAA, Astrodynamics Specialist Conference* (1981).
[26]A. Cummings, "The effects of grazing turbulent pipe-flow on the impedance of an orifice," Acta Acust. Acust. **61**(4), 233–242 (1986).
[27]N. Dickey, A. Selamet, and M. Ciray, "An experimental study of the impedance of perforated plates with grazing flow," J. Acoust. Soc. Am. **110**(5), 2360–2370 (2001).
[28]S.-H. Lee and J.-G. Ih, "Empirical model of the acoustic impedance of a circular orifice in grazing mean flow," J. Acoust. Soc. Am. **114**(1), 98–113 (2003).
[29]A. Goldman and C. Chung, "Impedance of an orifice under a turbulent boundary layer with pressure gradient," J. Acoust. Soc. Am. **71**(3), 573–579 (1982).
[30]A. Goldman and R. L. Panton, "Measurement of the acoustic impedance of an orifice under a turbulent boundary layer," J. Acoust. Soc. Am. **60**(6), 1397–1405 (1976).
[31]C. K. Tam and K. A. Kurbatskii, "Microfluid dynamics and acoustics of resonant liners," AIAA J. **38**(8), 1331–1339 (2000).
[32]K. A. Kurbatskii and C. K. Tam, "Micro-fluid dynamics of a resonant liner in a grazing flow," AIAA Paper, Vol. 1951 (2000).
[33]C. K. Tam, H. Ju, and B. E. Walker, "Numerical simulation of a slit resonator in a grazing flow under acoustic excitation," J. Sound Vib. **313**(3), 449–471 (2008).
[34]Q. Zhang, "Direct numerical investigation and reduced-order modeling of 3-D honeycomb acoustic liners," University of Illinois at Urbana-Champaign, 2014.
[35]E. Selamet, A. Selamet, A. Iqbal, and H. Kim, "Effect of flow on Helmholtz resonator acoustics: A three-dimensional computational study vs. Experiments," SAE Tech. Paper 0148-7191 (2011).
[36]C. Liu and Z. Ji, "Computational fluid dynamics-based numerical analysis of acoustic attenuation and flow resistance characteristics of perforated tube silencers," J. Vib. Acoust. **1362**, 021006 (2014).
[37]J. Su, J. Rupp, A. Garmory, and J. F. Carrotte, "Measurements and computational fluid dynamics predictions of the acoustic impedance of orifices," J. Sound Vib. **352**, 174–191 (2015).
[38]C. Malmary, S. Carbonne, Y. Auregan, and V. Pagneux, "Acoustic impedance measurement with grazing flow," in *AIAA Conference Paper* (2001).
[39]J.-M. Roche, F. Vuillot, L. Leylekian, G. Delattre, E. P. E. F. Simon, and E. Piot, "Numerical and experimental study of resonant liners aeroacoustic absorption under grazing flow," in *Proceedings of the 16th AIAA/CEAS Aeroacoustics Conference* (2010), No. 2010-3767.
[40]S. B. Pope, *Turbulent Flows* (Cambridge University Press, London, 2000), pp. 273–274.
[41]H. Fujita, "Turbulent flow in smooth and rough-walled square ducts," Trans. Jpn. Soc. Mech. Eng., Ser. B **45**, 197–207 (1979).
[42]W.-Y. Wu, S. Weinbaum, and A. Acrivos, "Shear flow over a wall with suction and its application to particle screening," J. Fluid Mech. **243**, 489–518 (1992).
[43]I. J. Sobey, "Laminar boundary-layer flow past a two-dimensional slot," J. Fluid Mech. **83**(1), 33–47 (1977).
[44]S. Smith, "Stokes flow past slits and holes," Int. J. Multiphase Flow **13**(2), 219–231 (1987).
[45]O. Tutty, "Flow in a tube with a small side branch," J. Fluid Mech. **191**, 79–109 (1988).
[46]A. Davis, "Shear flow disturbance due to a hole in the plane," Phys. Fluids A. **3**(3), 478–480 (1991).

15 February 2024 01:59:50